

**Mechanical Testing Program**  
**for Thermal Barrier Coating Development**

**NASA Lewis Research Center**

**Cooperative Agreement NCC3-187**

**Final Report**

C. V. Sidwell and T. A. Cruse  
Department of Mechanical Engineering  
Vanderbilt University  
Nashville, TN 37235

Report 96-0801

## TABLE OF CONTENTS

1. Introduction.....	1
2. Thermal Specimen Analysis .....	1
2.1 Goals of the Finite Element Analysis Effort .....	1
2.1.1 Existing Model .....	1
2.1.1.1 Finite Element Model Geometry .....	2
2.1.1.2 Material Properties.....	5
2.1.1.3 Elements and Meshing .....	5
2.1.1.4 Problems with Existing Model .....	5
2.1.2 Updated Model .....	6
2.1.2.1 Radius Definition .....	7
2.1.2.2 Application of Radius .....	12
2.2 Solution Methods.....	13
2.2.1 Transient Thermal Analysis .....	13
2.2.2 Thermal Stress Analysis.....	15
2.3 Analysis Results .....	16
2.3.1 Thermal Transient Results .....	17
2.3.2 Thermal Stress Results.....	17
2.3.3 Altered Substrate Stiffness Results .....	19
2.4 Convection Model .....	19
2.5 Convection Results .....	24
2.5.1 Experimental Discrepancies.....	24
2.5.2 Effect of TBC Thermal Conductivity .....	24
3. Adhesion Test Specimen Design .....	25
3.1 Purpose of Finite Element Analysis .....	25
3.2 Finite Element Model Generation .....	26
3.3 Solution Method .....	26
3.4 Results .....	27
4. Conclusions.....	31
Appendix A.....	33
References.....	43

## LIST OF FIGURES

Figure 1: Dimensions of TBC Specimen .....	2
Figure 2: Test Specimen Symmetries .....	3
Figure 3: Profile of Finite Element Model.....	4
Figure 4: Area of Stress Concentration on Original Model (without symmetry) .....	6
Figure 5: Profile of Radiused Corner.....	7
Figure 6: Typical Radius .....	8
Figure 7: Reference Numbers for Node Relocation.....	9
Figure 8: Movement of Nodes Along X-Axis.....	11
Figure 9: Movement of Midside Nodes.....	12
Figure 10: Finite Element Boundary Conditions .....	14
Figure 11: Location of Nodes of Interest.....	17
Figure 12: Experimental Cooling of Uncoated Angle Iron.....	20
Figure 13: Estimated Heat Transfer Coefficient .....	21
Figure 14: Convective Boundary Conditions.....	23
Figure 15: Adhesion Test Specimen .....	26
Figure 16: Tensile Stress vs. Radius at TBC - Pull-Bar Interface.....	28
Figure 17: Tensile Stress vs. Radius at TBC - Substrate Interface .....	29
Figure 18: Final Pull-Bar Design.....	30
Figure 19: Final Adhesion Specimen Design.....	31
Figure 20: Finite Element Mesh .....	34
Figure 21: Actual (Left) and Modeled (Right) Surface Temperatures at 10 Seconds.....	35
Figure 22: Temperature Contours at 240 Seconds.....	38
Figure 23: Non-convecting Model Temperatures vs. Time .....	39
Figure 24: Convecting Model Temperatures vs. Time .....	40
Figure 25: Finite Element Model of Adhesion Pull-bar.....	41

## LIST OF TABLES

Table 1: Coordinates Defining Profile Geometry (meters).....	4
Table 2: Material Properties .....	5
Table 3: Radii Through Thickness of Model (meters).....	9
Table 4: Approximate Radii of Actual Specimen (meters).....	10
Table 5: Parameters for Node Relocation.....	13
Table 6: Load Steps and Corresponding Time Points .....	14
Table 7: Load Steps Used For Stress Analysis .....	16
Table 8: New and Old Model Stresses (MPa) .....	18
Table 9: Linear Interpolation of Stress Due to True Radius (MPa).....	18
Table 10: Doubled Substrate Modulus Results (MPa) .....	19
Table 11: Piecewise-Linear Approximation of Heat Transfer Coefficient .....	21
Table 12: Application of Convection Cooling.....	22
Table 13: Altered Heat Transfer Coefficient (W/m <sup>2</sup> K) .....	24
Table 14: Effect of Decreased TBC Thermal Conductivity.....	25
Table 15: Sample Load Step File .....	36
Table 16: Transient Solution Commands .....	37
Table 17: Sample Input File for Adhesion Pull-bar Analysis .....	42

## 1. Introduction

This reported effort was performed in support of an experimental effort to characterize the mechanical properties of a specific thermal barrier coating (TBC) system. The effort primarily focused on the thermal testing of an “angle-iron” specimen being tested in the burner rig facility at NASA Lewis Research Center under the direction of Dr. Robert A. Miller. A second and much smaller effort concerned a new design for an adhesion test pull-bar. Both sets of analyses reported herein consisted of finite element models of thermal barrier coated specimens. The TBC used in the analyses is zirconia ( $\text{ZrO}_2$ ) that has been partially stabilized with 7 - 8% (by weight) yttria ( $\text{YrO}_2$ ).

The first analysis was performed on the angle-iron specimen designed and tested at NASA Lewis Research Center. This specimen simulated a fatigue critical location on a TBC coated diesel engine piston head. The finite element analysis was used to characterize the sensitivity of the specimen to changes in leading edge radius, substrate stiffness, and TBC conductivity. In addition, the finite element model was updated in order to predict the effects of free convection on the response of the specimen.

The second analysis was used to design a pull-bar to test the adhesion strength of the TBC to the substrate. The final design produces an improved tensile stress distribution along the interface of the TBC and the substrate, as compared to the ASTM C633-79 standard test method.

## 2. Thermal Specimen Analysis

### 2.1 *Goals of the Finite Element Analysis Effort*

The burner rig experiments on the TBC specimen attempt to simulate the thermomechanical conditions on a critical piston head location that lead to spallation of the TBC. A finite element model was generated to determine the experimental stresses based on thermographic and thermocouple data supplied by NASA. As part of the study, the sensitivity of the stresses to the radius of the corner in the middle of the steel angle, the stiffness of the substrate, and the thermal conductivity of the thermal barrier coating was assessed.

#### 2.1.1 Existing Model

The finite element model was based on an idealization of the geometry of the experimental specimen. The specimen is a piece of angle-iron 0.045m in length, with the exterior of the bar coated with a thermal barrier coating, nominally 60 mils thick. The dimensions of the specimen are shown in Figure 1. The specimen was sprayed at an orientation of 45 degrees to each face of the steel angle. This produced the angle on the edge of the TBC with respect to the steel substrate.

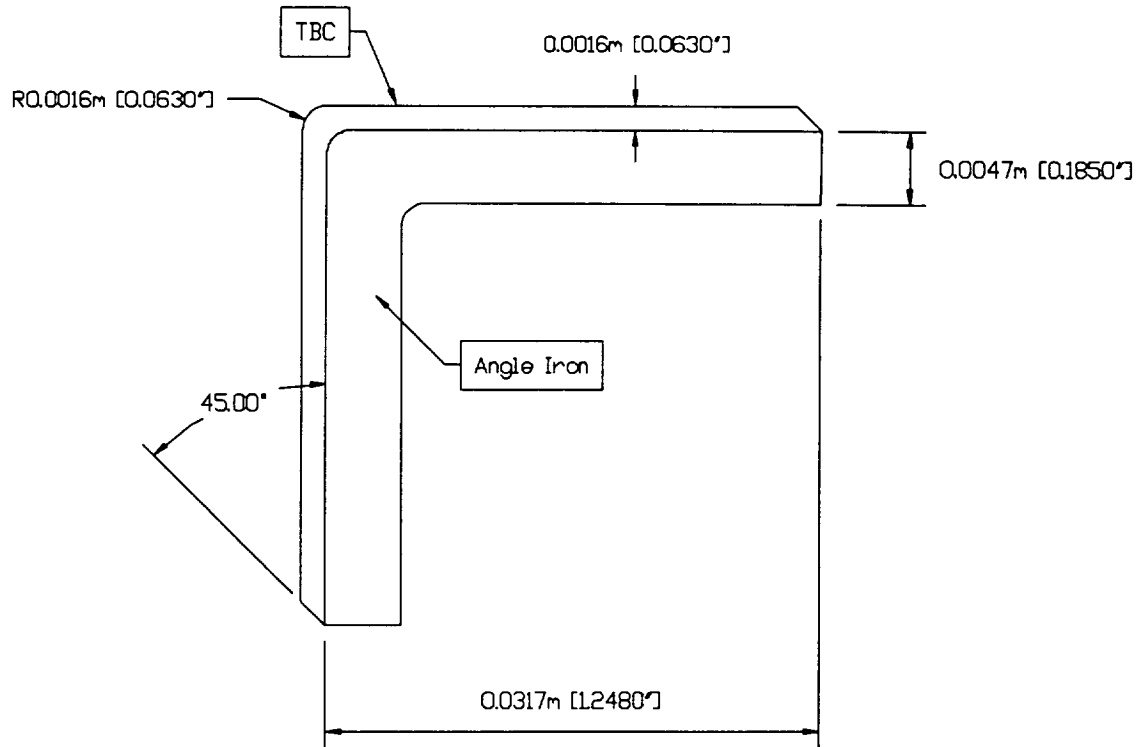


**Figure 1: Dimensions of TBC Specimen**

#### ***2.1.1.1 Finite Element Model Geometry***

Since the two sides of the specimen have the same dimensions, the specimen is plane symmetric about a plane that bisects the corner of the specimen. Also, the specimen is assumed to be symmetric about its mid-length where the heat input from the burner rig is applied. The symmetric finite element model is shown in Figure 2.

The actual test specimen was not symmetric about its mid-length. An additional length of uncoated bar extended below the coated section.. Axial heat conduction along the length of the specimen was ignored for modeling simplicity. Temperature data was averaged for the two sides of the hot spot. The effect of this additional bar is discussed in later sections.

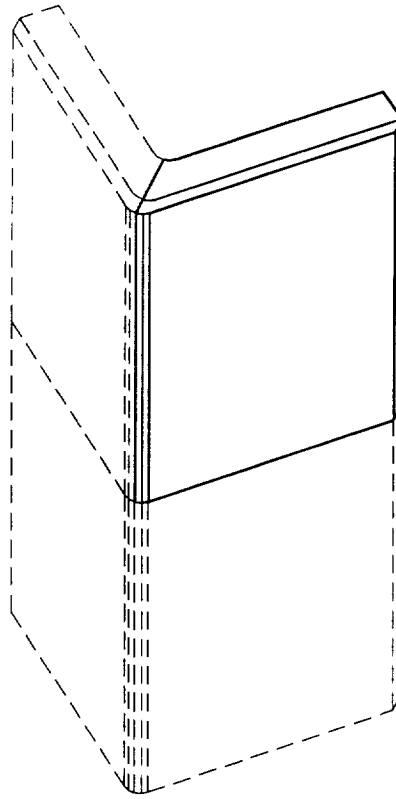


**Figure 2: Test Specimen Symmetries**

Symmetry was used to reduce the complexity of the three-dimensional model. Only one quarter of the specimen was modeled, which significantly reduced computational time. The profile of the geometric model used for the finite element analysis is shown in Figure 3. The numbers in the figure correspond to coordinates shown in Table 1.

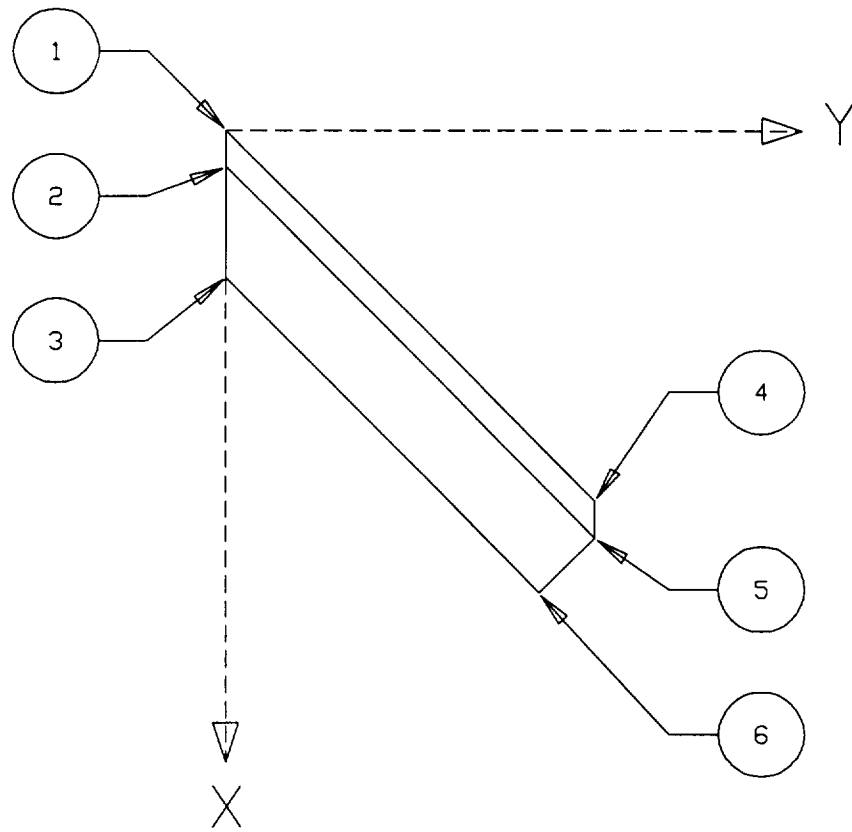


**Figure 3: Profile of Finite Element Model**

**Table 1: Coordinates Defining Profile Geometry (meters)**

Numb	X	Y	Z
1	0	0	0
2	0.0022	0	0
3	0.0089	0	0
4	0.0225	0.0225	0
5	0.0247	0.0225	0
6	0.0280	0.0191	0

### 2.1.1.2 Material Properties

The material properties of the steel substrate and the thermal barrier coating are shown in Table 2. Where  $E$  is the modulus of elasticity,  $\alpha$  is the coefficient of thermal expansion,  $\rho$  is the density,  $\kappa$  is the thermal conductivity,  $c$  is the thermal capacity, and  $\nu$  is Poisson's ratio.

**Table 2: Material Properties**

Prope	Steel Substrate	TBC
$E$	207 GPa	13.5 GPa
$\alpha$	12.3 $\mu\text{mm/mm}$	10 $\mu\text{mm/mm}$
$\rho$	7850 $\text{kg/m}^3$	5236 $\text{kg/m}^3$
$\kappa$	46.7 W/m K	0.9 W/m K
$c$	456.4 J/kg K	582 J/kg K
$\nu$	0.3	0.13

### 2.1.1.3 Elements and Meshing

Two different element types were used during the analysis. For the transient thermal analysis, a 20-node thermal solid brick element was used, SOLID90 in ANSYS.<sup>1</sup> This is a brick with one node at each corner and one midside node on each edge. For the thermal stress analysis, however, a different element type was chosen. A 20-node structural solid element was used in this case, SOLID95 in ANSYS.<sup>2</sup>

Mapped meshing was utilized in order to attain a desired mesh pattern of brick shaped elements throughout the specimen. Two elements were used through the thickness of the TBC for accuracy. The steel substrate would also have two elements through its thickness. Along the face of the TBC, the smallest elements were used near the zone of heating, while farther away from the heated zone, larger elements are used. The mapped mesh resulted in four elements through the thickness, seven elements along the profile of the specimen, and twelve elements along the axis of the specimen. In total, 336 elements were used. The mesh can be seen in Figure 20 in Appendix A.

### 2.1.1.4 Problems with Existing Model

As can be seen in Figure 4, the model had a perfectly sharp corner at the apex of the angle (circled portion of figure). This sharp corner exaggerated the normal or interface stress concentration at the interface of the TBC and the steel substrate directly under the applied heat. The sharp corner was removed in subsequent modeling in order to simulate the effect of radius on the interface normal stress.

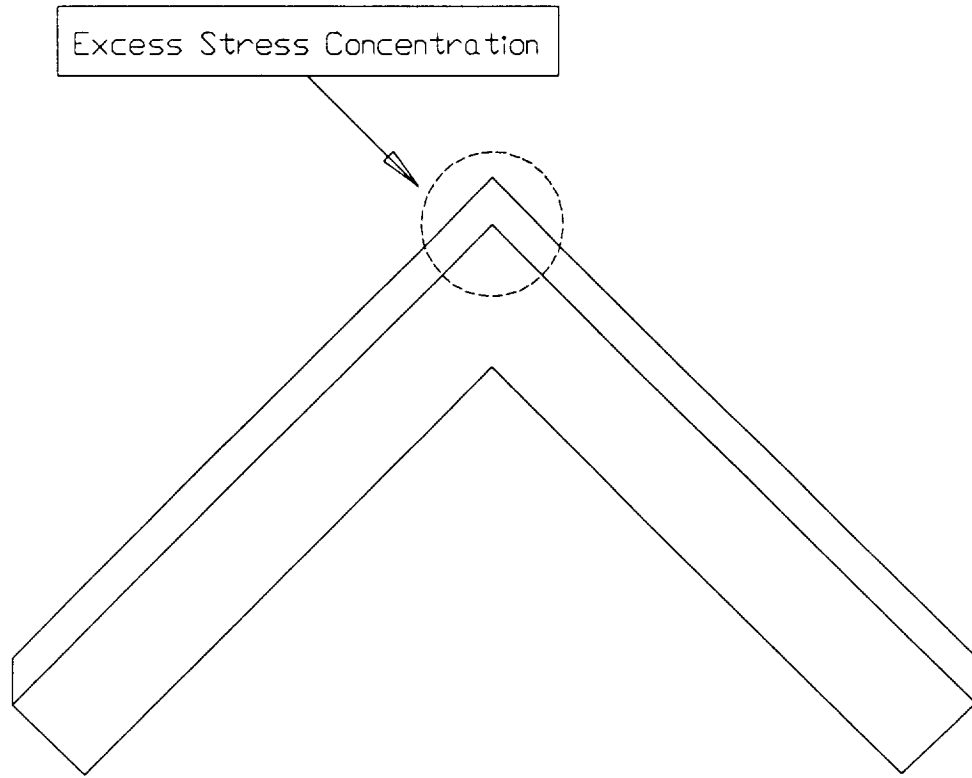


**Figure 4: Area of Stress Concentration on Original Model (without symmetry)**

### **2.1.2 Updated Model**

The geometry of the revised finite element model was identical to that of the original model, except for the region along the exterior corner of the angle iron. A finite radius at the corner reduces the stress concentration. The radius of the corner was approximated such that only elements located along the x-axis would be altered. This restriction limited our ability to match the actual specimen. However, the approach allowed us to use the same input thermal boundary conditions as before - a significant savings in effort. The nodes along the x-axis as well as the first row of midside nodes were relocated to describe the radiused corner, as can be seen in Figure 5.

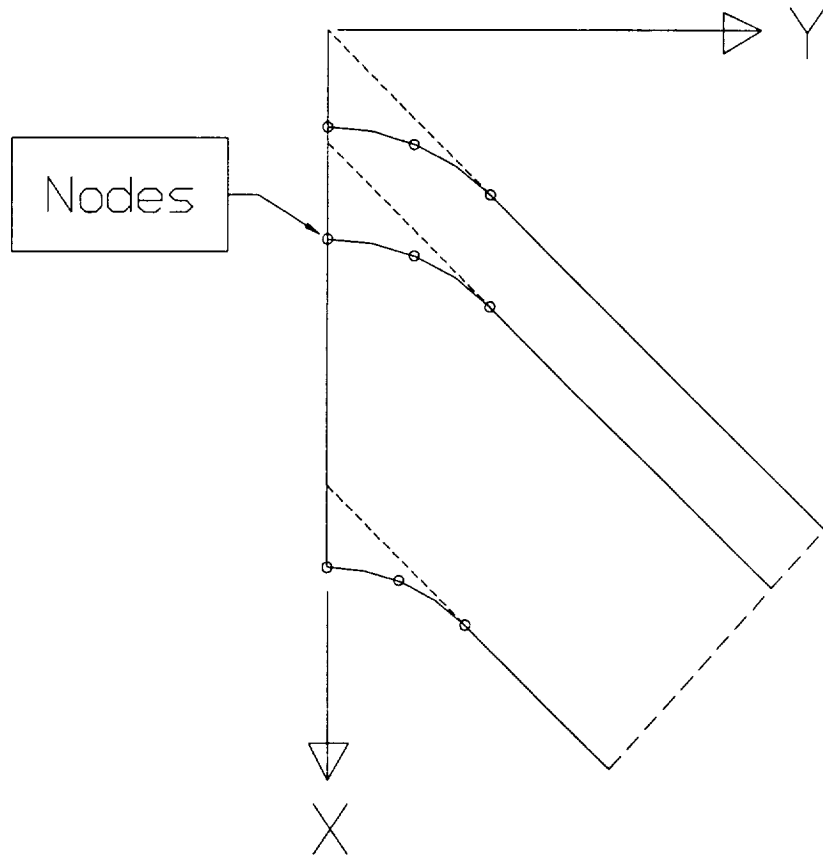


**Figure 5: Profile of Radiused Corner**

#### **2.1.2.1 Radius Definition**

The radius was defined by the length of a line perpendicular to the original element edge at the location of the first inter-element node and the location where this line crosses the x-axis. Figure 6 shows a typical radius. The radii were calculated by the formula

$$r = y\sqrt{2} \quad [1]$$

where  $y$  is the y-coordinate of the first inter-element node of the layer of interest. Figure 7 shows the locations of the reference numbers, while Table 3 lists the radii used through the thickness of the model.

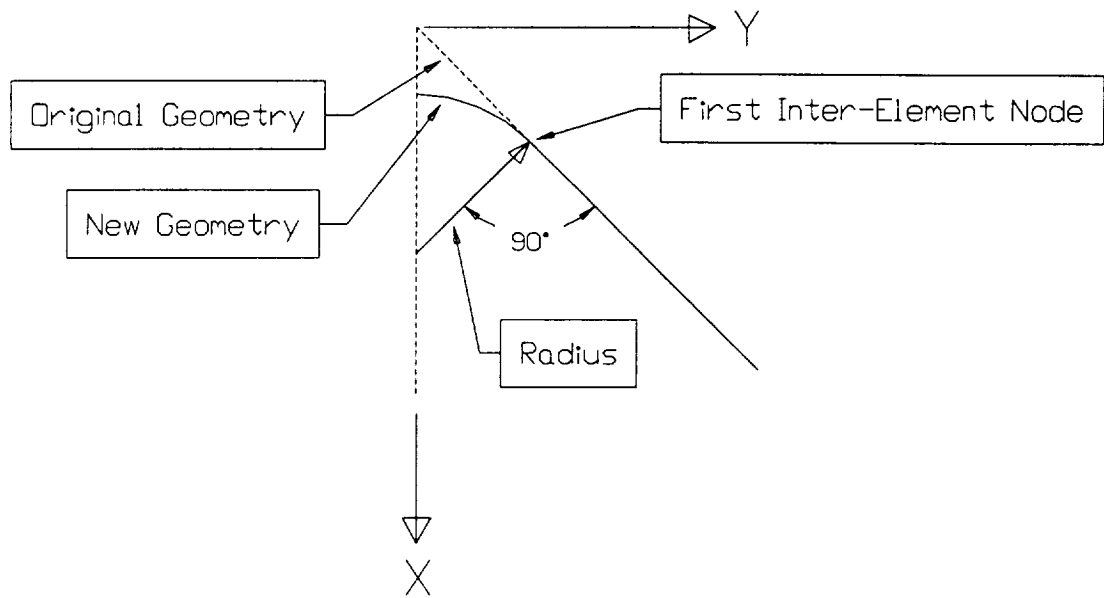


**Figure 6: Typical Radius**

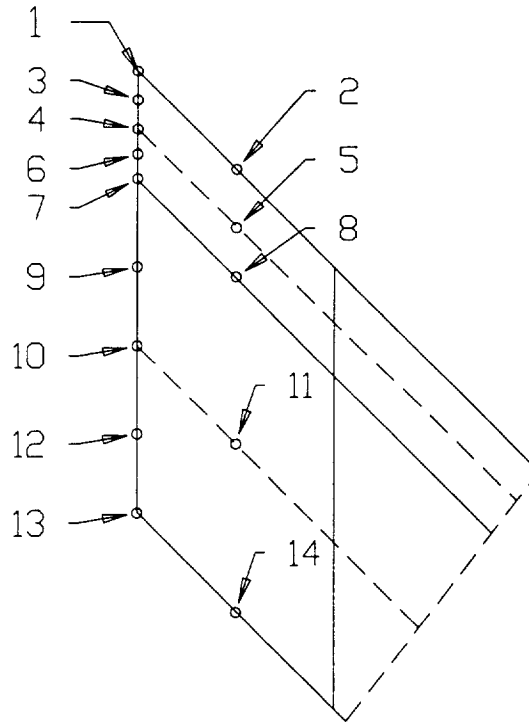


**Figure 7: Reference Numbers for Node Relocation**

**Table 3: Radii Through Thickness of Model (meters)**

Reference No.	Radius
1	0.0045457
2	0.0045457
3	0.0045457
4	0.0045457
5	0.0045457
6	0.0045457
7	0.0045457
8	0.0045457
9	0.004374
10	0.0042022
11	0.0042022
12	0.0040305
13	0.0038588
14	0.0038588

The model radii are greater than those on the actual specimen. The comparison of radii can be seen in Table 4. The finite element stress analysis results show sensitivity of the peak interfacial stress, normal to the interface, to the modeled radius. The finite element stresses were interpolated over the radius variable and were found to be close to the results originally given for no radius. It is strongly suggested that the angle-iron specimen and the piston component be given a more generous radius to reduce the peak interfacial stress concentration.

**Table 4: Approximate Radii of Actual Specimen (meters)**

Reference No.	FEM Radius	Specimen Radius
1	0.0045457	0.000762
7	0.0045457	0.000254
13	0.0038588	0.00203

The nodes that lie on the x-axis (reference numbers 1,3,4,6,7,9,10,12, and 13 in Figure 7) were relocated by the formula

$$x_{1r} = 2x_1 - x_i - r \quad [2]$$

where the variables are illustrated in Figure 8.

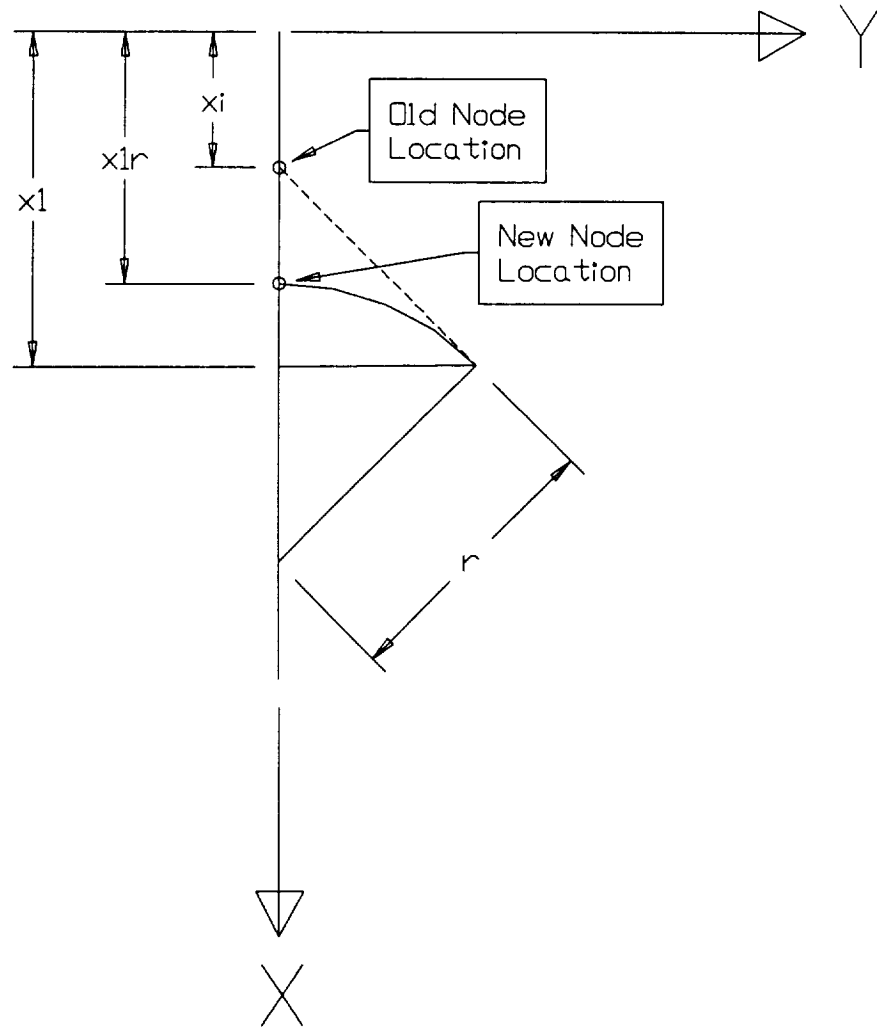


**Figure 8: Movement of Nodes Along X-Axis**

The midside nodes (reference numbers 2,5,8,11, and 14 in Figure 7), were moved by the formula

$$x_{2r} = 2x_1 - x_i - \sqrt{r^2 - y_2^2} \quad [3]$$

where the variables are illustrated in Figure 9.

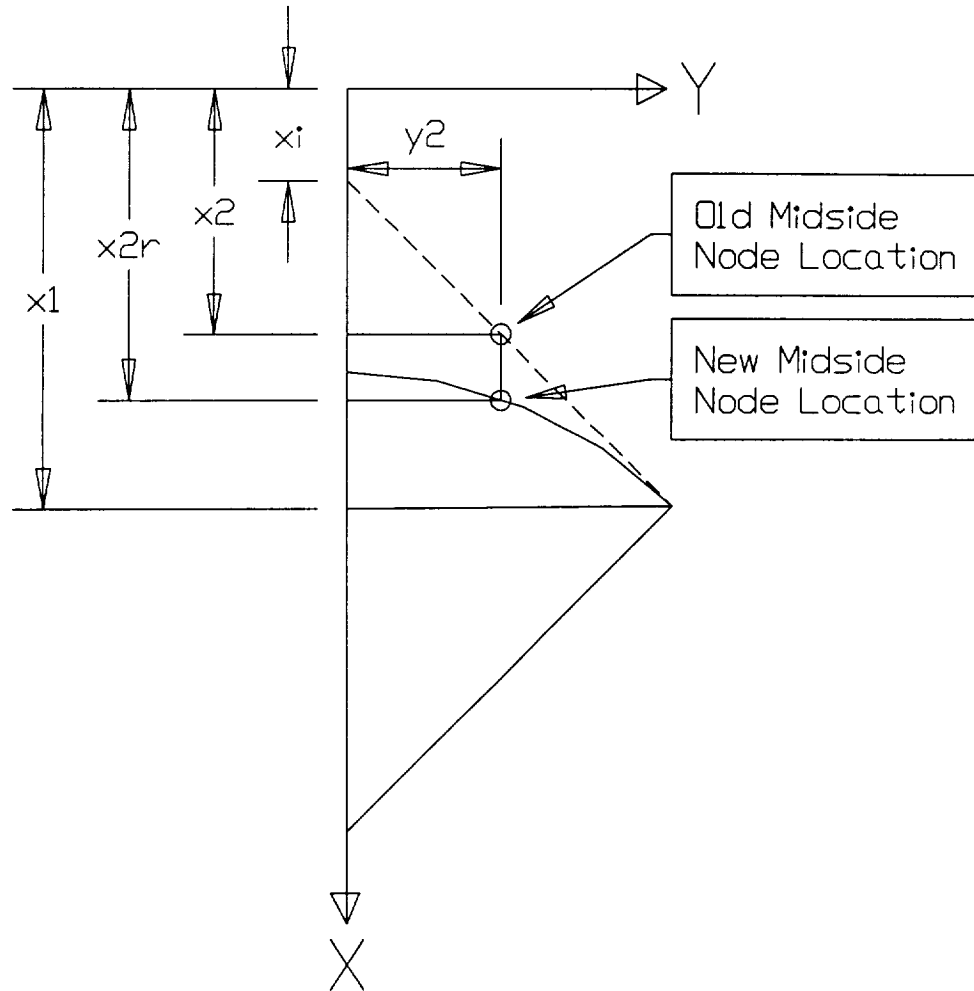


**Figure 9: Movement of Midside Nodes**

#### **2.1.2.2 Application of Radius**

Although the necessity of changing the geometry was obvious, the method of altering the finite element model was not. Since the thermal loads are applied to specific node numbers on the front and back face of the model, it was not feasible to redraw the geometry or to create an entirely new model, as this would result in different node numbers. This prevented the alteration of the solid model, which would necessitate remeshing. The nodes of interest would need to be individually moved to their new locations.

When a mesh is generated in ANSYS, the nodes are automatically numbered in an order appropriate to the model. If the mesh is deleted and the model is remeshed, the node numbering starts where the previous meshing operation had left off. For example, if the first meshing operation generates nodes numbered one to ten and the mesh is then deleted, the remeshing will start with node number eleven and continue sequentially from that point.

In order to move the nodes, the finite element model was disassociated from the solid model. The command MODMSH,NOCHECK was issued. This deactivated solid model cross-reference

checking so that the nodes could be moved independent of the geometry of the solid model, since the model geometry did not include the desired radius at the vertex of the specimen.

The nodes were moved using the NMODIF command and the new locations calculated previously. The new node locations and the parameters involved are shown in Table 5, where the variables refer to Figure 8 and Figure 9.

**Table 5: Parameters for Node Relocation**

Ref. No.	$x_1$	$x_i$	$r$	$x_2$	$y_2$	$x_{1r}$	$x_{2r}$
1	0.0032143	0.0000000	0.0045457	--	--	0.0018829	--
2	0.0032143	0.0000000	0.0045457	0.0016071	0.0016071	--	0.0021760
3	0.0037643	0.0005500	0.0045457	--	--	0.0024329	--
4	0.0043143	0.0011000	0.0045457	--	--	0.0029829	--
5	0.0043143	0.0011000	0.0045457	0.0027071	0.0016071	--	0.0032760
6	0.0048643	0.0016500	0.0045457	--	--	0.0035329	--
7	0.0054143	0.0022000	0.0045457	--	--	0.0040829	--
8	0.0054143	0.0022000	0.0045457	0.0038071	0.0016071	--	0.0043760
9	0.0069679	0.0038750	0.0043740	--	--	0.0056868	--
10	0.0085214	0.0055000	0.0042022	--	--	0.0073406	--
11	0.0085214	0.0055000	0.0042022	0.0071594	0.0016094	--	0.0076610
12	0.0100750	0.0072250	0.0040305	--	--	0.0088945	--
13	0.0116290	0.0089000	0.0038588	--	--	0.0104992	--
14	0.0116290	0.0089000	0.0038588	0.0105120	0.0016116	--	0.0108520

## 2.2 Solution Methods

Two separate analyses were performed to analyze the stresses in the bar due to heating and cooling. The first was the transient thermal analysis that determined the temperatures through the specimen during the heating and cooling cycles. The second was a quasi-static stress analysis that used the temperatures determined in the previous solution to determine the stresses produced by thermal expansion.

### 2.2.1 Transient Thermal Analysis

The time-dependent thermal loading was modeled using experimentally determined temperature constraints on the front and back nodes of the model. The specimen was heated for 300 seconds, then allowed to cool for another 360 seconds.

The transient thermal loading was determined from data obtained from NASA Lewis.<sup>3</sup> The temperatures measured from the front and back faces of the specimen during the experiment were converted into nodal temperature constraints on the finite element model. A sample temperature profile is given as Figure 21 in Appendix A. The specimen was subjected to heating for 300 seconds, then allowed to cool. The thermal loading consisted of temperature constraints on the front and back side of the model that varied with time and position on the face. Figure 10 shows the boundary conditions for the transient thermal analysis. These loads were set up in a file specifically for use in the ANSYS finite element program.

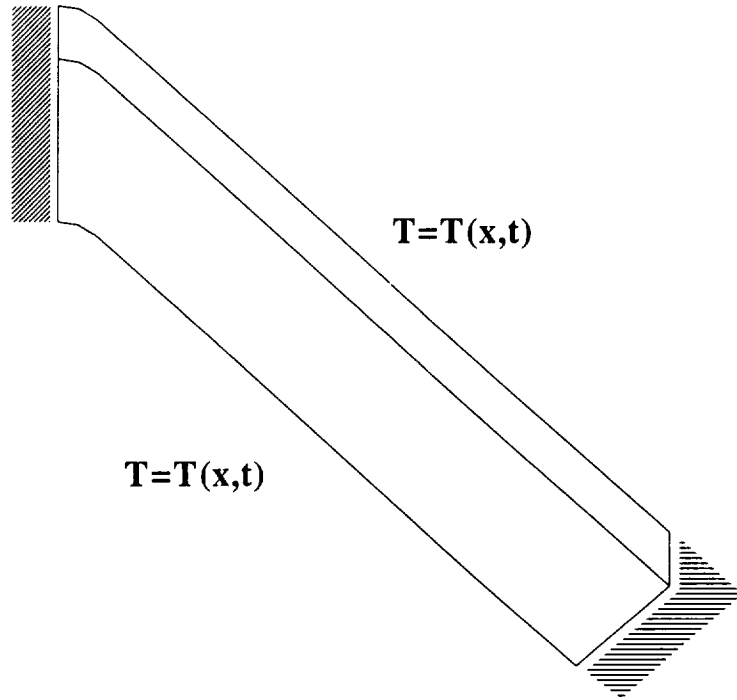


**Figure 10: Finite Element Boundary Conditions**

The transient temperature load is approximated by piecewise-linear segments. Each segment is referred to as a load step. That is, the first time point was specified with its corresponding temperature profile. This would be referred to as load step number one. The second time step was specified with its corresponding temperature profile. This would be load step two. For the purpose of analysis, ANSYS performs a linear interpolation of temperature between these two time points. A sample load step file is given as Table 15 in Appendix A.<sup>4</sup>

Sixteen load steps were used. The first eleven include heating while load steps twelve through sixteen constitute the cooling phase. Table 6 shows the load steps and their corresponding time points.

**Table 6: Load Steps and Corresponding Time Points**

Load Step	Time* (s)	Loading
--	0	--
1	2	Heating
2	5	Heating
3	10	Heating
4	20	Heating
5	30	Heating
6	45	Heating
7	60	Heating
8	120	Heating
9	180	Heating
10	240	Heating
11	300	Heating
12	301	Cooling
13	310	Cooling
14	330	Cooling
15	345	Cooling
16	660	Cooling

\* - Time at end of load step

Each load step, with its corresponding temperature field, was saved as a unique file. The load step file for the first time point contained commands that instructed the program to use all the load step files of interest.

A transient solution was performed that included all load steps. The transient thermal solution produced a thermal results file which contained the temperatures throughout the model for the time period of interest (0 - 660 seconds). The necessary commands to perform this transient solution are shown as Table 16 in Appendix A.

### 2.2.2 Thermal Stress Analysis

The temperature gradient through the TBC produces significant stresses in the model. A quasi-static analysis was used to model the stresses. The stresses were statically determined at time points of interest, thus approximating the stresses due to the transient loading.

A temperature distribution at a specific time point from the previous thermal analysis was used to perform a quasi-static stress analysis. The temperatures throughout the model, at the chosen time point, were assumed to be static. This static temperature field was used to calculate the stresses. The result was an approximation of stress throughout the model for the given time point.

Instead of finding the stresses at every time point, specific time points were selected as representative of the behavior of the specimen. These time points are shown in Table 7.

**Table 7: Load Steps Used For Stress Analysis**

<b>Load Step</b>	<b>Time* (s)</b>	<b>Loading</b>
1	2	Heating
2	5	Heating
3	10	Heating
4	20	Heating
11	300	Heating
12	301	Cooling
13	310	Cooling

\* - Time at end of load step

The two time regions shown (steps 1-4 and 11-13) include the times of greatest interest. The first four load steps span the time of significant temperature change, when the heat is initially applied to the specimen. Significant stresses are present here, due to the high temperature in the TBC and low temperature in the substrate. The last three load steps cover the removal of the heat source, the initial cool-down phase.

### **2.3 Analysis Results**

The area of greatest interest is the interface of the TBC and the substrate at the exterior corner, directly under the heated zone. The stresses at this point can be observed by utilizing the results for the node at that point, node 1872. Also, for the purpose of comparing the difference in stress levels for the revised and original specimen model geometry, a node at the surface of the TBC was chosen, node 2953. The node locations can be seen in Figure 11.

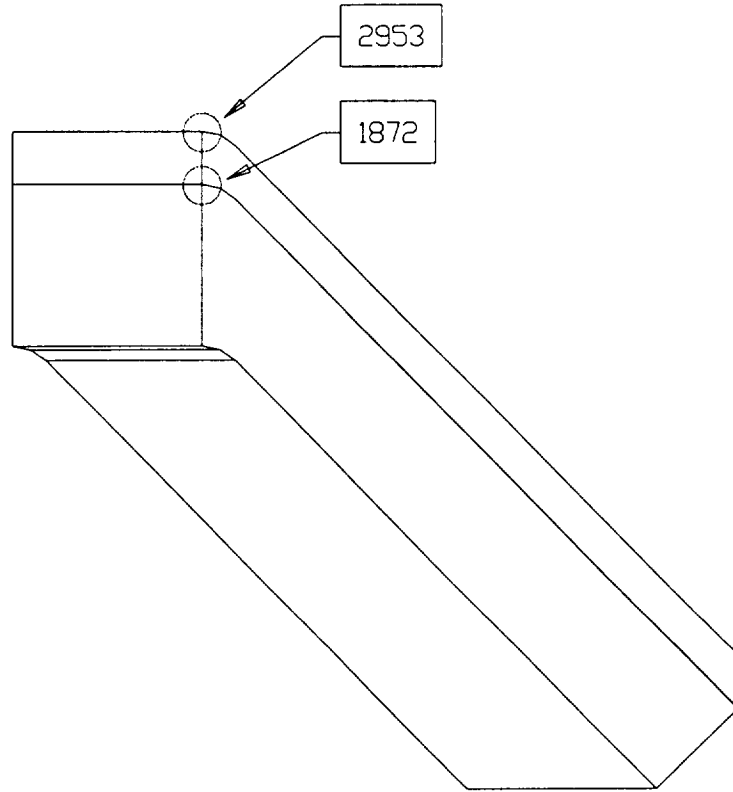


**Figure 11: Location of Nodes of Interest**

### **2.3.1 Thermal Transient Results**

The graphical results of the thermal transient analysis are shown in Figure 22 in Appendix A, in the form of contour plots of temperature. The maximum temperature is just over 1000 C. Note the significant thermal gradient across the thickness of the TBC. The gradient is on the order of 400 C over a thickness of 0.16 cm. The gradient in the substrate is on the order of 100 C over 0.47 cm.

### **2.3.2 Thermal Stress Results**

The radius at the vertex significantly affected the stresses. Table 8 shows the stresses (x, y, and z) in the original (no radius) and revised (with radius) models for the time points of interest at each node of interest. Once again, node 2953 is on the surface of the TBC directly under the heat source. Node 1872 is at the interface between the TBC and the steel substrate, under the heated zone.

The approximate stresses due to the actual radii of the experimental specimen are shown in Table 9. These are based on a linear interpolation of the actual radii and the radii used in the finite element model.

**Table 8: New and Old Model Stresses (MPa)**

**Node 2953**

<b>Time (sec)</b>	<b>Sx (old)</b>	<b>Sx (new)</b>	<b>Change</b>	<b>Sy (old)</b>	<b>Sy (new)</b>	<b>Change</b>	<b>Sz (old)</b>	<b>Sz (new)</b>	<b>Change</b>
2	6.9341	2.7853	-4.1488	-65.344	-80.536	-15.192	-98.196	-97.142	1.054
5	6.9494	3.4792	-3.4702	-45.921	-60.799	-14.878	-94.918	-96.918	-2
10	7.7629	3.7409	-4.022	-50.771	-64.946	-14.175	-98.92	-101.1	-2.18
20	7.1192	3.534	-3.5852	-42.385	-54.261	-11.876	-87.956	-89.835	-1.879
300	4.7773	2.1687	-2.6086	-27.525	-36.159	-8.634	-45.869	-47.376	-1.507
301	3.5114	1.8708	-1.6406	-12.72	-19.031	-6.311	-25.413	-27.701	-2.288
310	-1.2832	-1.0414	0.2418	7.4866	8.9365	1.4499	28.807	28.16	-0.647

**Node 1872**

<b>Time (sec)</b>	<b>Sx (old)</b>	<b>Sx (new)</b>	<b>Change</b>	<b>Sy (old)</b>	<b>Sy (new)</b>	<b>Change</b>	<b>Sz (old)</b>	<b>Sz (new)</b>	<b>Change</b>
2	30.122	16.11	-14.012	7.3277	4.2955	-3.0322	6.443	5.5005	-0.9425
5	37.304	22.647	-14.657	10.081	5.6741	-4.4069	2.9832	4.651	1.6678
10	39.633	24.135	-15.498	12.526	7.1534	-5.3726	12.24	11.917	-0.323
20	35.568	20.825	-14.743	15.46	10.843	-4.617	13.167	13.075	-0.092
300	22.722	10.57	-12.152	21.441	19.245	-2.196	27.215	25.706	-1.509
301	17.649	7.9824	-9.6666	20.256	18.623	-1.633	25.867	24.887	-0.98
310	-5.0143	-6.2465	-1.2322	13.781	15.177	1.396	24.957	22.78	-2.177

**Table 9: Linear Interpolation of Stress Due to True Radius (MPa)**

**Node 2953**

<b>Time (sec)</b>	<b>Sx (old)</b>	<b>Sx (new)</b>	<b>Sx*</b>	<b>Sy (old)</b>	<b>Sy (new)</b>	<b>Sx*</b>	<b>Sz (old)</b>	<b>Sz (new)</b>	<b>Sx*</b>
2	6.934	2.785	6.239	-65.344	-80.536	-67.891	-98.196	-97.142	-98.019
5	6.949	3.479	6.368	-45.921	-60.799	-48.415	-94.918	-96.918	-95.253
10	7.763	3.741	7.089	-50.771	-64.946	-53.147	-98.920	-101.100	-99.285
20	7.119	3.534	6.518	-42.385	-54.261	-44.376	-87.956	-89.835	-88.271
300	4.777	2.169	4.340	-27.525	-36.159	-28.972	-45.869	-47.376	-46.122
301	3.511	1.871	3.236	-12.720	-19.031	-13.778	-25.413	-27.701	-25.797
310	-1.283	-1.041	-1.243	7.487	8.937	7.730	28.807	28.160	28.699

**Node 1872**

<b>Time (sec)</b>	<b>Sx (old)</b>	<b>Sx (new)</b>	<b>Sx*</b>	<b>Sy (old)</b>	<b>Sy (new)</b>	<b>Sx*</b>	<b>Sz (old)</b>	<b>Sz (new)</b>	<b>Sx*</b>
2	30.122	16.110	29.339	7.328	4.296	7.158	6.443	5.501	6.390
5	37.304	22.647	36.485	10.081	5.674	9.835	2.983	4.651	3.076
10	39.633	24.135	38.767	12.526	7.153	12.226	12.240	11.917	12.222
20	35.568	20.825	34.744	15.460	10.843	15.202	13.167	13.075	13.162
300	22.722	10.570	22.043	21.441	19.245	21.318	27.215	25.706	27.131
301	17.649	7.982	17.109	20.256	18.623	20.165	25.867	24.887	25.812
310	-5.014	-6.247	-5.083	13.781	15.177	13.859	24.957	22.780	24.835

\* - Interpolated to approximate stress due to radii of actual specimen.

The stresses dropped considerably due to the radiused vertex in the model. In some cases, the stresses were roughly half of the old model stresses. The maximum stress is produced at roughly 10 seconds; the TBC is relatively hot, but the steel is still at ambient temperature. However, the interpolated stresses for the actual radius show very little change from the sharp corner model. The radii on the actual specimen are closer to the perfectly sharp model than the radiused model. Significant life enhancement in the piston component and in the angle-iron specimen could be achieved by using a larger radius at this critical location.

### 2.3.3 Altered Substrate Stiffness Results

The finite element model was run with a doubled substrate modulus of elasticity. The doubled modulus approximated an increased substrate thickness by increasing the section modulus (EI) of the substrate. The model was run with a doubled modulus because the modulus is easier to change than thickness in the finite element model.

The results of the analysis with the doubled modulus are shown in Table 10. The modulus of the substrate has little effect on the stresses. A 100% change in modulus result in a 1% change in stress (at the maximum stress in the table). Therefore, changing the thickness of the substrate would have little effect on the stress levels.

**Table 10: Doubled Substrate Modulus Results (MPa)**  
(Normalized to largest value in table.)

Node 1872									
Time	Sigma X			Sigma Y			Sigma Z		
	(old)	(new)	Change*	(old)	(new)	Change*	(old)	(new)	Change*
10	0.855521	0.870935	-2%	0.395348	0.367054	7%	0.320327	0.280198	13%
300	0.27229	0.277489	-2%	0.947143	0.936197	1%	1	0.98568	1%

\* (old-new)/old

### 2.4 Convection Model

Convection cooling was included in the model in order to update the model to match the current experimental conditions. The heat transfer coefficient was determined by matching the experimental cooling curve data of an existing specimen, since no accurate value for the heat transfer coefficient was available and it is unrealistic to analytically derive a suitable value

Cooling data of the uncoated angle iron material used as a substrate in the current specimen was available. Correlating a finite element model to the cooling curve of this uncoated angle iron would produce the most realistic value of the heat transfer coefficient. The measured cooling curve of the uncoated iron bar is shown in Figure 12.

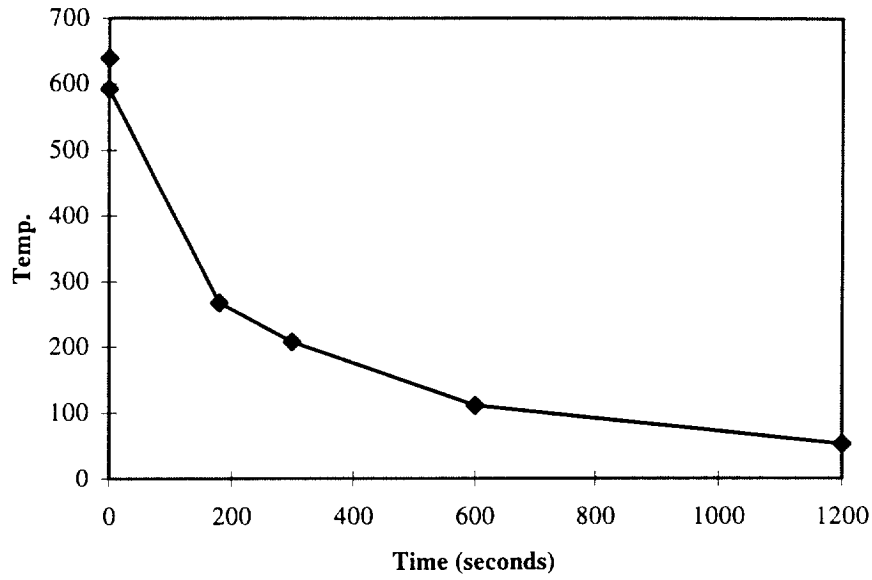


**Figure 12: Experimental Cooling of Uncoated Angle Iron**

It was necessary to have an initial estimate of a heat transfer coefficient. This estimate was used to obtain a finite element solution and then altered accordingly to obtain an updated estimate of the coefficient. The coefficient was updated until the cooling curve of the model sufficiently matched the cooling curve of the angle iron. The flow over the specimen was assumed to be laminar. This allowed for the use of an empirically derived approximation for the heat transfer coefficient:

$$h_c = 1.07 \left( \frac{\Delta T}{x} \right)^{\frac{1}{4}} \quad [4]$$

where  $h_c$  is the heat transfer coefficient for natural convection in  $\text{W/m}^2\text{K}$ .<sup>5</sup> An average heat transfer coefficient over the entire body was determined by the formula<sup>6</sup>:

$$\overline{h_c} = \frac{1}{A} \int_0^A h_c dA \quad [5]$$

Then combining Equations [4] and [5], and integrating:

$$\overline{h_c} = \frac{1.07}{L} \left( \frac{4}{3} \right) \Delta T^{\frac{1}{4}} L^{\frac{3}{4}} \quad [6]$$

The result was the average heat transfer coefficient as a function of temperature. This provided an initial estimate for the heat transfer coefficient. The actual coefficient was

determined by correlating the finite element model to the measured angle iron cooling curve. The graph of the initial estimate of the average heat transfer coefficient versus temperature can be seen in Figure 13.

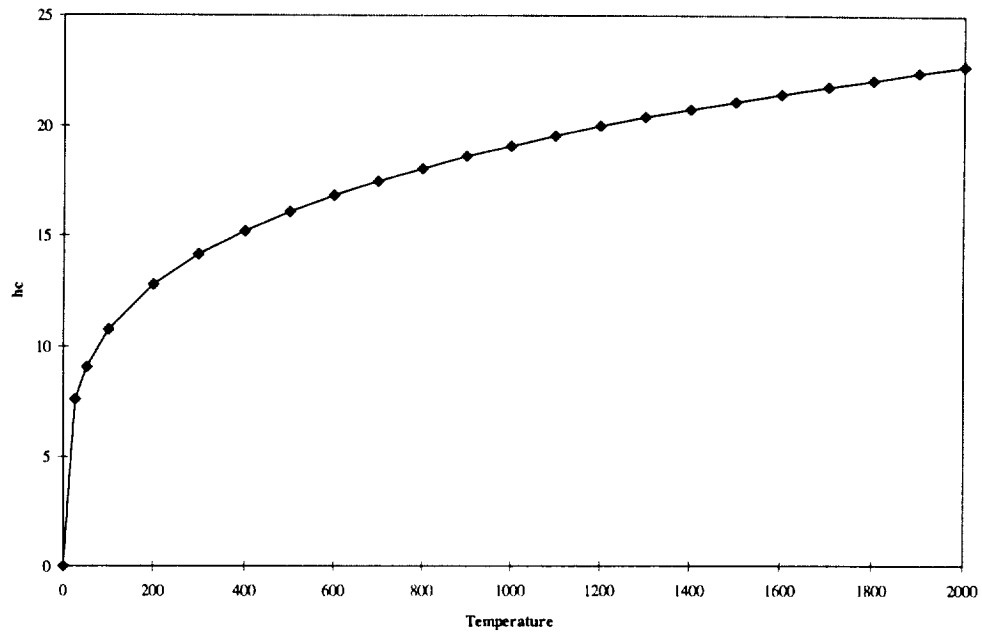


**Figure 13: Estimated Heat Transfer Coefficient**

The heat transfer coefficient curve was approximated by five linear segments. These segments defined a piecewise-linear approximation that would be utilized by ANSYS during the transient thermal analysis. The six points that define the five segments are listed in Table 11.

**Table 11: Piecewise-Linear Approximation of Heat Transfer Coefficient**

Temp	Hc
0	0
50	9
300	14
500	16
900	19
2000	23

The finite element model convects heat for the entire cycle, to accurately model the response of the experimental specimen. Since temperatures were constrained on the front face during heating, the specimen was allowed to convect on the front face after the heat source was removed and on the back face for the entire cycle. Table 12 shows the convection application. Note that additional load steps were introduced to allow the specimen to cool to ambient temperature.

**Table 12: Application of Convection Cooling**

Load Step	Time* (s)	Front Face	Back Face
--	0	--	--
1	2	Heating	Convection
2	5	Heating	Convection
3	10	Heating	Convection
4	20	Heating	Convection
5	30	Heating	Convection
6	45	Heating	Convection
7	60	Heating	Convection
8	120	Heating	Convection
9	180	Heating	Convection
10	240	Heating	Convection
11	300	Heating	Convection
12	301	Convection	Convection
13	310	Convection	Convection
14	330	Convection	Convection
15	345	Convection	Convection
16	400	Convection	Convection
17	600	Convection	Convection

\* - Time at end of load step

The boundary conditions for the convective cooling finite element model are shown in Figure 14.

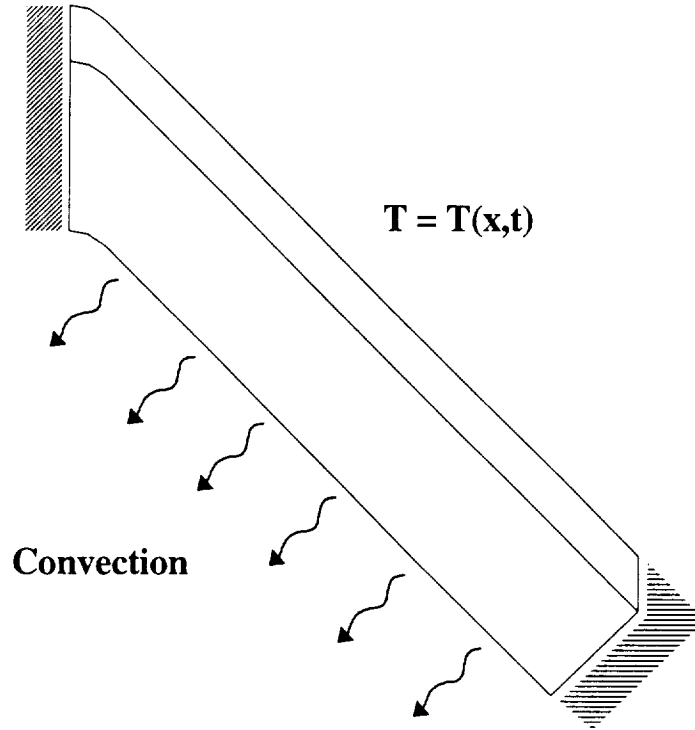


**Figure 14: Convective Boundary Conditions**

In the process of trying to correlate the finite element model of an uncoated bar with the experimental cooling data, there was an apparent discrepancy between the finite element model and the experiment. When asked if anything had been left out of the analysis, NASA replied that there was an additional seven inches of uncoated iron bar beneath the coated section. This extra bar would significantly effect the thermal response of the specimen.

Since the convective cooling is a function of the exposed area and the heat transfer coefficient, it was possible to approximate the effect of the additional area by appropriately increasing the value of the heat transfer coefficient. The surface area of the coated section is  $0.00617 \text{ m}^2$ , while the surface area of the coated section and the uncoated section is  $0.0224 \text{ m}^2$ . The altered heat transfer coefficient was then calculated:

$$h_{new} = \frac{h_{old} A_{new}}{A_{old}} \quad [7]$$

where  $h$  is the heat transfer coefficient and  $A$  is the surface area.

The final values of the heat transfer coefficient, including the additional area, are shown in Table 13.

**Table 13: Altered Heat Transfer Coefficient (W/m<sup>2</sup>K)**

time	hc (old)	Area(old)	Area(new)	hc (new)
0	0	0.0062	0.0286	0
50	27	0.0062	0.0286	125
300	42	0.0062	0.0286	194
500	48	0.0062	0.0286	222
900	54	0.0062	0.0286	250
2000	66	0.0062	0.0286	306

## **2.5 Convection Results**

The temperature profiles of both the non-convecting and convecting models can be seen in Figure 23 and Figure 24 in Appendix A. The top curve on the both temperature profile figures is the temperature at the surface of the TBC, directly under the heated zone. The temperature profile of this location on the model is exactly the same for the non-convecting and convecting models since the temperatures are constrained in both cases. The remaining curves show the temperature profiles of locations through the thickness of the specimen.

### **2.5.1 Experimental Discrepancies**

The discrepancies between the convecting and non-convecting models can be attributed to two significant experimental factors: the heat sink behavior of the test fixture and specimen, and the existence of unintended forced convection. Unfortunately, the actual configuration of the experimental apparatus was not revealed until late in the finite element analysis; time would not allow the generation of a new model.

Below the coated section of the steel angle, there are seven inches of uncoated steel angle. This uncoated section acts as a heat sink, which creates a thermal flux along the length of the bar. Worse yet, the steel angle specimen is bolted to a large metal mounting plate. The connection between the specimen and the mounting plate covers a large area on the back face of the specimen, which allows heat to flow from the specimen to the mounting plate. This heat sink effect creates a thermal flux that has a significant effect on the thermal response of the coated section of the specimen. The heat transfer coefficient was altered to account for the uncoated section of steel angle, as previously discussed.

The finite element model was assumed to cool by free convection. The actual experimental apparatus consisted of a large air extraction duct that was located behind the specimen during heating. Presumably, this duct carried away the exhaust of the heating flame. The air movement created by the duct would cause the specimen to cool by forced convection, which would allow the specimen to cool much faster than if it were only cooled by free convection.

### **2.5.2 Effect of TBC Thermal Conductivity**

The effect of changing the thermal conductivity of the TBC was predicted using the convection cooling finite element model. The value of the conductivity was decreased from 0.9 W/m\*K to 0.7 W/m\*K. The change caused the temperature at the interface to increase more slowly during heating, but the effect on the maximum temperature level was small. The

decreased thermal conductivity means that the temperature gradient across the TBC is greater during heating. Table 14 shows the temperatures for the two cases at the location of interest.

**Table 14: Effect of Decreased TBC Thermal Conductivity**

<b>Node 1872</b>			
<b>Time</b>	<b>k=0.9 Temp</b>	<b>k=0.7 Temp</b>	<b>Change</b>
2	6	3	-51%
5	62	42	-32%
10	146	111	-24%
20	274	222	-19%
30	364	304	-16%
45	455	393	-14%
60	514	454	-12%
120	634	586	-8%
180	660	621	-6%
240	651	614	-6%
300	661	622	-6%
301	661	622	-6%
305	630	600	-5%
320	489	474	-3%
345	351	344	-2%
400	191	190	0%

### **3. Adhesion Test Specimen Design**

#### **3.1 Purpose of Finite Element Analysis**

The purpose of this phase of the TBC analysis was to design a specimen to determine the adhesion strength of the TBC to the substrate. The intent is to spray the top of a steel cylinder with TBC, then bond a “pull-bar” to the exposed face of the TBC. Figure 15 shows a rendering of the specimen configuration. The goal of the design was to produce a specimen that provides a uniform tensile stress at the interface of the TBC and the substrate while reducing the effect of the stress singularity at the edge of the pull bar.

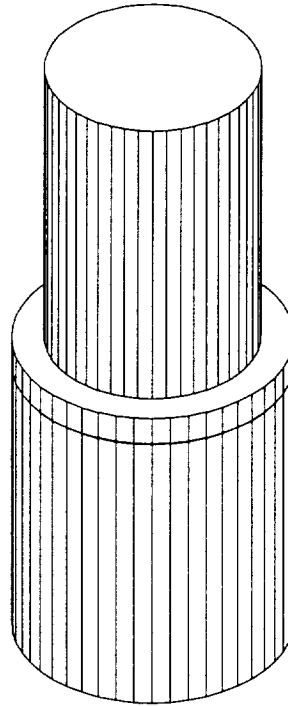


**Figure 15: Adhesion Test Specimen**

The radius of the pull bar was assumed to be 0.333 inches. Initially, the thickness of the TBC was 0.050 inches. This provided a radius to thickness ratio of 6.66. This ratio is the critical dimension. The scale of the specimen can be varied as needed, but the ratio governs the behavior of the specimen.

### ***3.2 Finite Element Model Generation***

A finite element model was generated that utilized the axisymmetry of the specimen. This resulted in a two-dimensional finite element model. The model was meshed with two-dimensional eight-node structural solid elements. The location at which the edge of the pull-bar contacted the surface of the TBC was specified as a stress concentration location and meshed accordingly. The loading consisted of an applied tensile stress on the top of the pull-bar, while the base of the steel substrate was constrained with no displacement. The finite element model can be seen in Figure 25 in Appendix A.

### ***3.3 Solution Method***

In an effort to attain the desired tensile stress distribution, many pull-bar profiles were analyzed. These ranged from a simple cylindrical profile to a complex curved profile defined by a B-spline. Since it was necessary to analyze a number of different profiles and each analysis was identical except for a few keypoint locations, the model generation and solution commands were entered into an input file. The input file was then executed from the ANSYS interactive interface which allowed the model generation and analysis to proceed without any interaction

from the user. This not only streamlined the process of analyzing the effect of different profiles, it ensured consistency between analyses. A sample input file is given as Table 17 in Appendix A.

### **3.4 Results**

A number of different features were included in the pull-bar design in an attempt to satisfy the requirements for the specimen. The evolution of the pull-bar, including these features, can be seen in Figure 16 and Figure 17. Figure 16 plots the tensile stress versus radius for the TBC - pull-bar interface. Figure 17 plots the tensile stress versus radius for the TBC - substrate interface.

In Figure 16, Plot A shows the tensile stress distribution for a cylindrical pull-bar. Stress is minimum at the center and the singularity at the edge is significant. Plot B includes a profile and central hole to attempt to flatten the stress distribution. Plot C deepens the central hole, which increases the stress in the center, resulting in a more uniform stress distribution in the central region. Plot D includes a very small notch at the edge of the pull-bar to reduce the effect of the stress singularity. Plot E utilizes a larger notch which significantly reduces the effect of the stress concentration. Plot F uses the same pull-bar design as Plot E, but the thickness of the TBC is doubled to 0.100 inches. The ratio of radius to TBC thickness is decreased to 3.33, which increased the effect of the stress singularity. Figure 17 uses the same evolutionary sequence as Figure 16, but the tensile stresses are at the TBC - substrate interface. Notice that once the profile and central hole are included, the shape of the distribution is relatively insensitive to other features (except TBC thickness). The magnitude of the maximum stress does change, however. To ensure the proper failure at the TBC - substrate interface, the maximum stress at this interface should be as close as possible to the magnitude of the stress in the center of the TBC - pull-bar interface. Note that in Plot E for both figures, the central stress is approximately equal. Plot F shows the effect of increasing the thickness of the TBC. The thicker TBC tends to round off the distribution, making it less uniform.

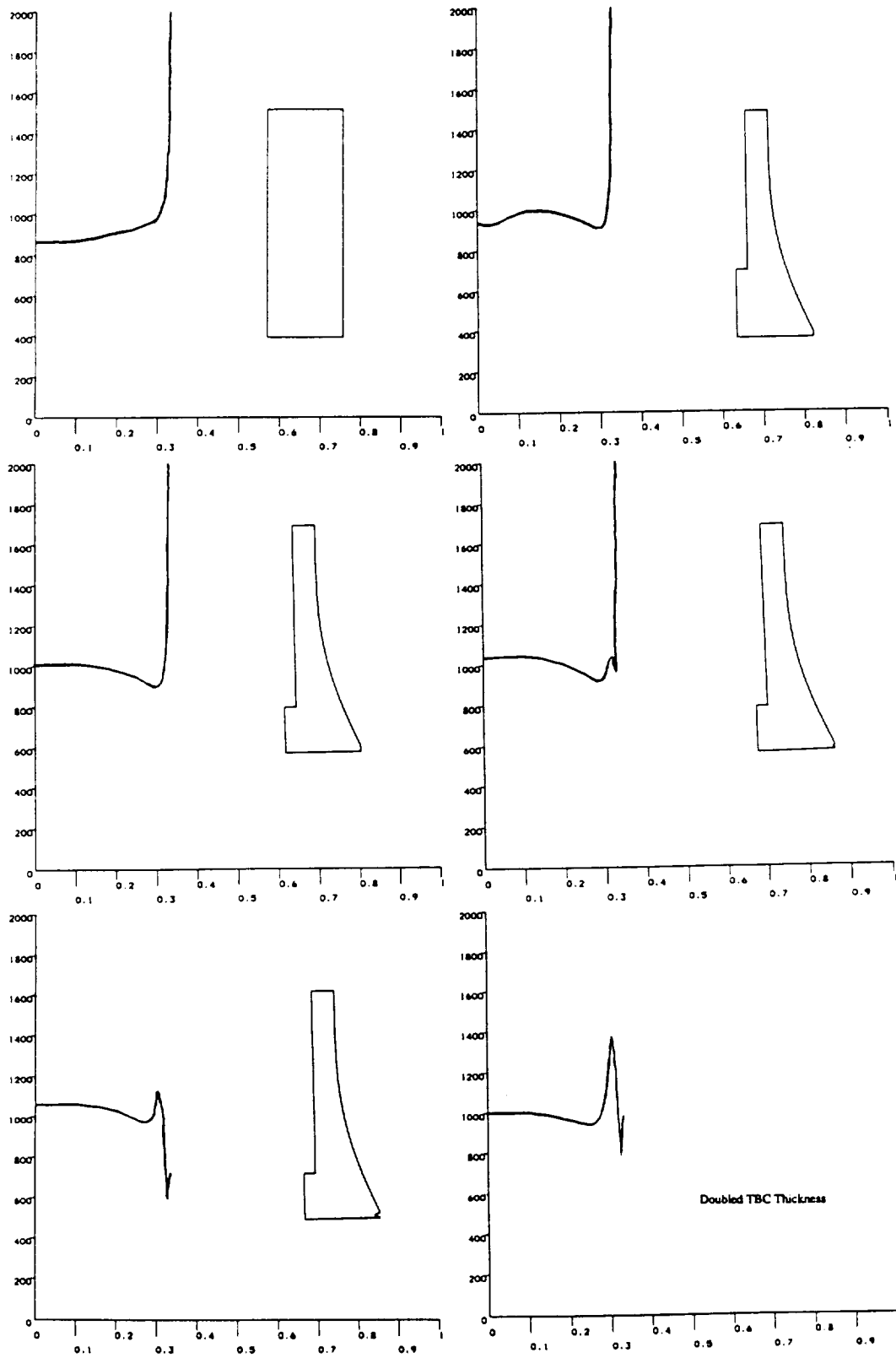


**Figure 16: Tensile Stress vs. Radius at TBC - Pull-Bar Interface**

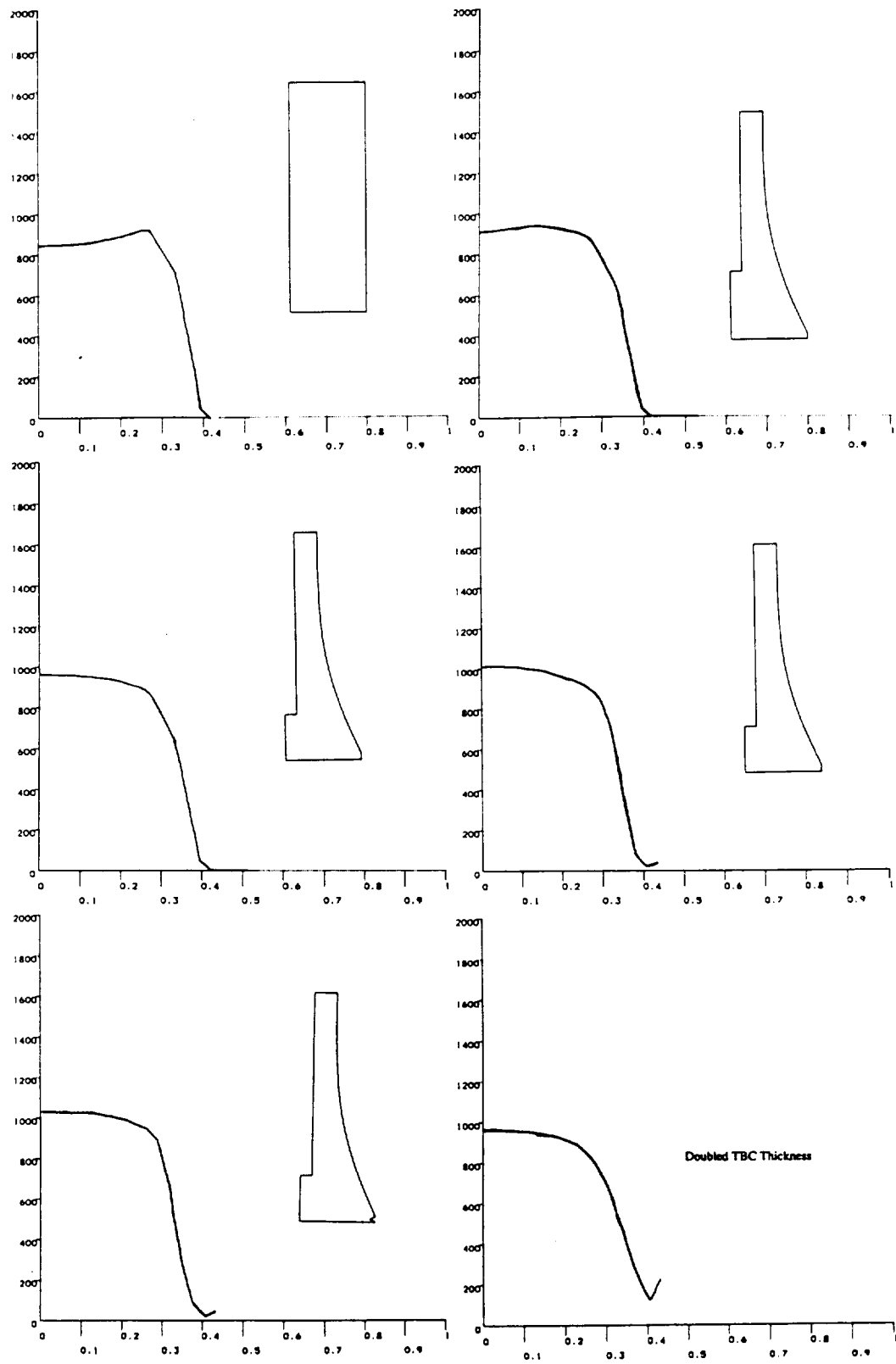


**Figure 17: Tensile Stress vs. Radius at TBC - Substrate Interface**

None of the designs provides a truly uniform distribution and a removed singularity, but the design used for Plot E in Figure 16 and

Figure 17 is the closest approximation. The final design can be seen in Figure 18 and Figure 19. A final CAD rendering of the specimen was reviewed with a machinist to establish a machinable configuration. The figures shown herein are nominal representations of the notch configuration.

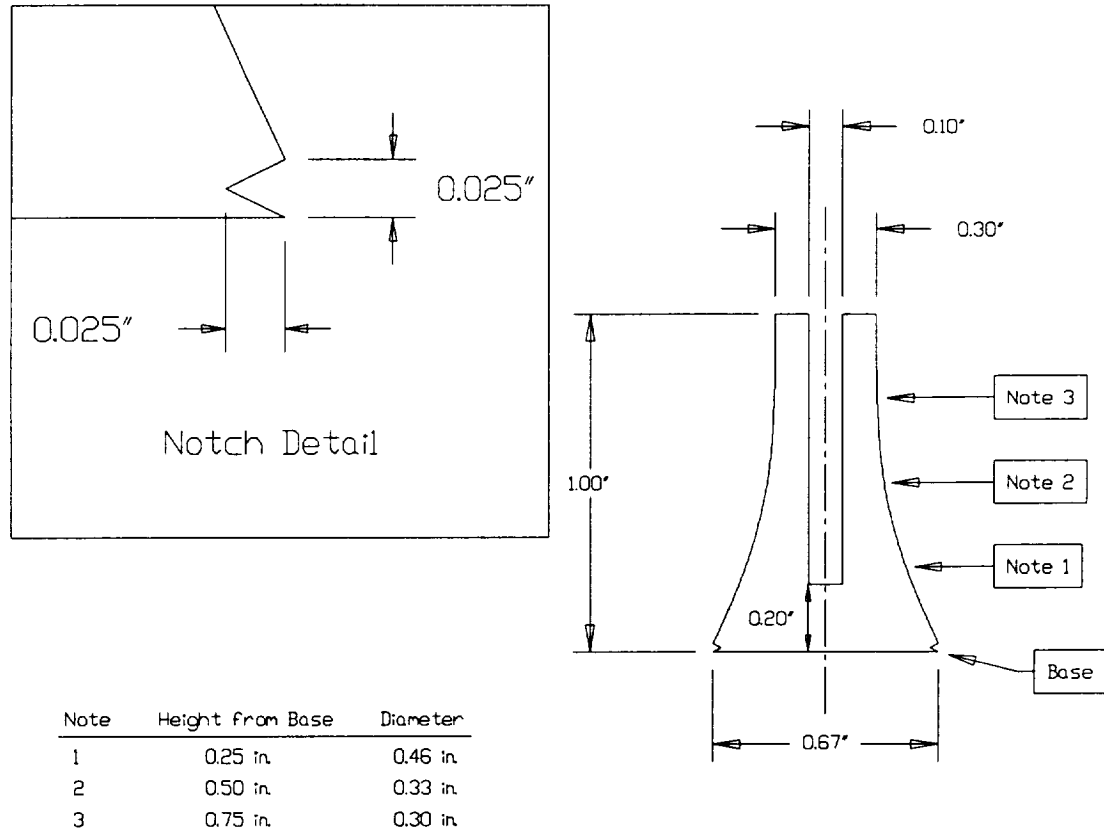


**Figure 18: Final Pull-Bar Design**

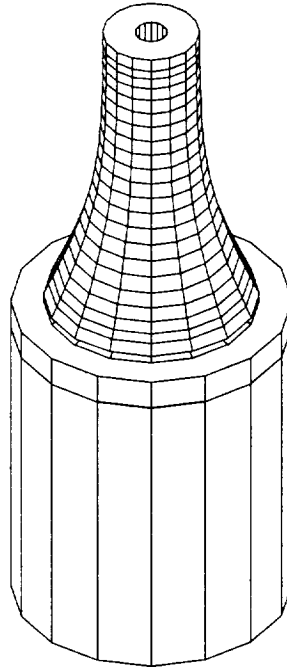


**Figure 19: Final Adhesion Specimen Design**

#### **4. Conclusions**

The first analysis of the TBC coated angle iron was performed with temperatures constrained on both the front and back faces of the finite element model. A finite radius was applied to the vertex of the angle iron which reduced the stress levels at the interface of the TBC and the substrate approximately 50%. Therefore, it seems possible that the TBC failure on the diesel engine piston head can be avoided by applying a radius to the edge of interest.

Changing the modulus of the steel substrate had very little effect on the response of the specimen. The modulus of the steel substrate is approximately 20 times greater than the modulus of the TBC. In essence, the substrate acts relatively rigid during deformation. Increasing the modulus of the substrate only makes it more stiff, which has little effect on the overall deformation or stress state.

Convection cooling was included in the finite element model of the TBC coated angle iron. The heat transfer coefficient was determined by correlating a finite element model to the known cooling behavior of an uncoated section of steel angle. The response of the coated specimen is reasonably approximated by the finite element model that included convection. Exact agreement is not possible due to uncertainties in the experimental apparatus.

The effect of reducing the thermal conductivity of the TBC was simulated. The thermal conductivity was reduced approximately 22%. This caused the specimen to heat up more slowly, producing a greater thermal gradient.

Finally, a quasi-optimal design was generated for an adhesion strength test specimen. The purpose of the specimen is to measure the tensile adhesion strength of the TBC to the steel substrate. The specimen was designed to provide an approximately constant distribution of stress along the interface between the TBC and the substrate while reducing the effect of the stress singularity caused by the edge of the specimen.

## **APPENDIX A**

### **Additional Figures**

**Figure 20: Finite Element Mesh**

```

ANSYS 5.0.2
FEB 26 1996
15:48:40
PLOT NO. 1
ELEMENTS
MAT NUM
XV = 0.299E-11
YV = 0.422E16
ZV = 0.90630E
DIST = 0.02167E
XE = 0.014E
YE = 0.0112E
ZF = 0.022E
E25=90
CENTROID HIDDEN

```

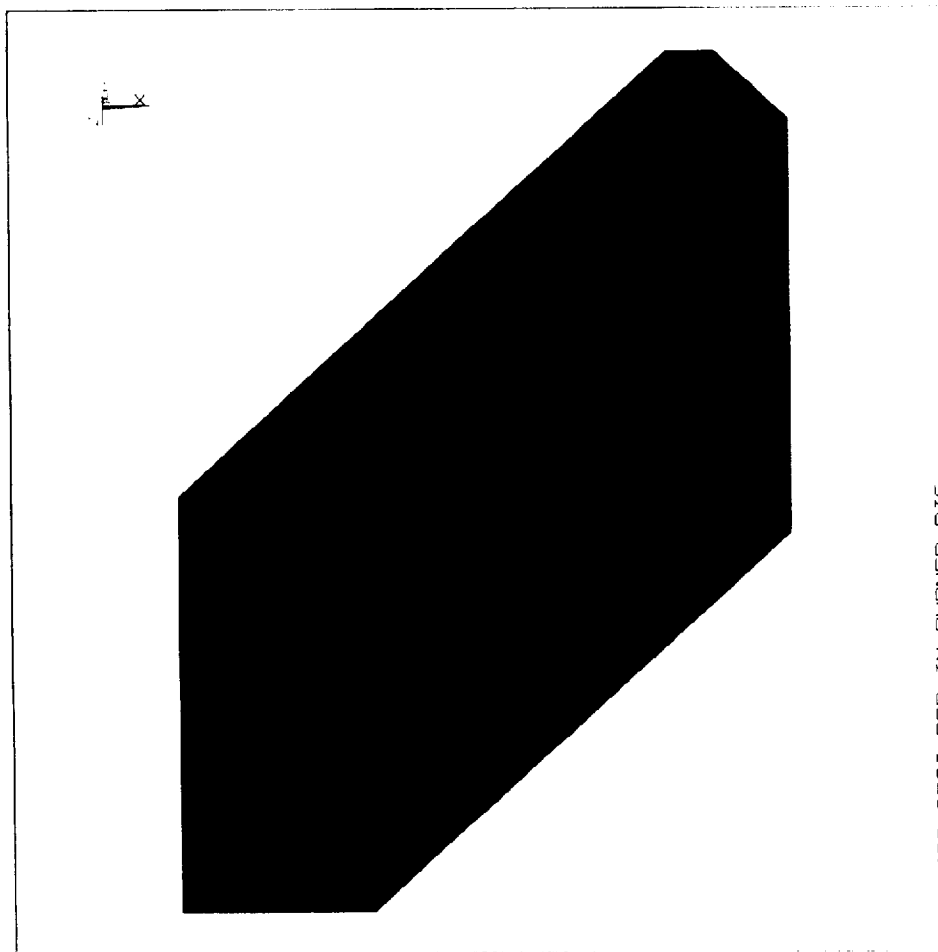


Figure 21: Actual (Left) and Modeled (Right) Surface Temperatures at 10 Seconds

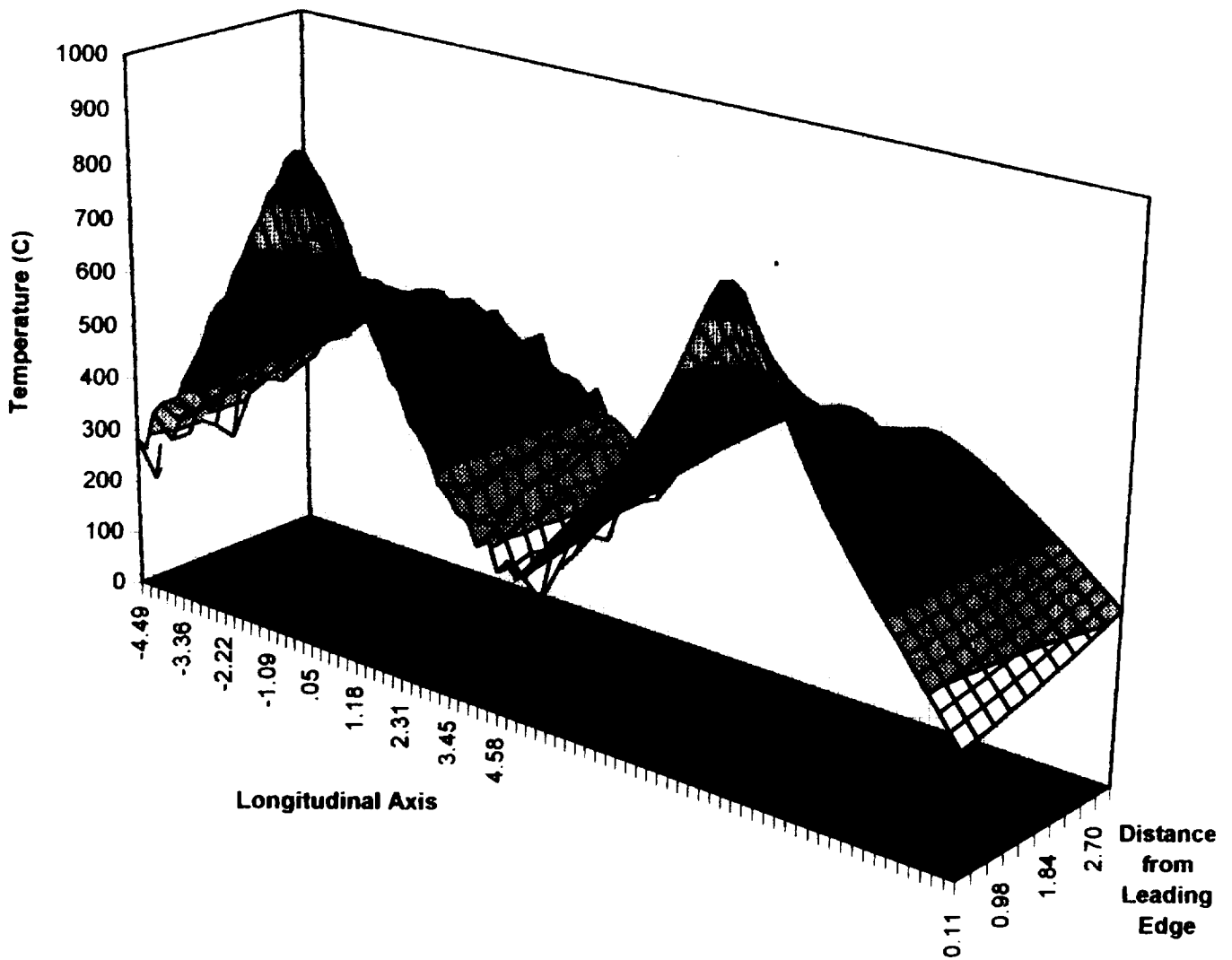


Table 15: Sample Load Step File

```

/COM,ANSYS REVISION 5.0          A      10:25:43      10/28/1994
/NOPR
/TITLE,NASA TBC TEST BAR IN FURNACE RIG
/LSNUM= 1
AUTOTS,ON
DELTIM, 0.100000000      , 0.000000000E+00, 0.000000000E+00,OFF
KBC, 0
KUSE, 0
TIME, 2.00000000
TREF, 0.000000000E+00
ALPHAD, 0.000000000E+00
BETAD, 0.000000000E+00
DMPRAT, 0.000000000E+00
TIMINT,ON ,THER
TINTPAR,R5.0, 5.000000000E-03,,,
TINTPAR,R5.0, 0.500000000      , 0.500000000      , 0.200000003
CRPLIM, 0.100000000
NCNV, 1, 0.000000000E+00, 0, 0.000000000E+00, 0.000000000E+00
LNSRCH,OFF
NEQIT, 25
PRED,OFF ,OFF
ERESX,DEFA
OUTPR,BASI, LAST,
ACEL, 0.000000000E+00, 0.000000000E+00, 0.000000000E+00
OMEGA, 0.000000000E+00, 0.000000000E+00, 0.000000000E+00, 0
DOMEGA, 0.000000000E+00, 0.000000000E+00, 0.000000000E+00
CGLOC, 0.000000000E+00, 0.000000000E+00, 0.000000000E+00
CGOMEG, 0.000000000E+00, 0.000000000E+00, 0.000000000E+00
DCGOME, 0.000000000E+00, 0.000000000E+00, 0.000000000E+00
IRLF, 0
D, 1873,TEMP, 0.000000000E+00
D, 1877,TEMP, 0.000000000E+00
D, 1878,TEMP, 0.000000000E+00
D, 1879,TEMP, 0.000000000E+00
D, 1880,TEMP, 0.000000000E+00
D, 1881,TEMP, 0.000000000E+00
D, 1882,TEMP, 0.000000000E+00
D, 1883,TEMP, 0.000000000E+00
.
.
(Repeated Commands Not Shown.)
.
D, 2953,TEMP, 720.
D, 2957,TEMP, 499.
D, 2961,TEMP, 510.
D, 2962,TEMP, 522.
D, 2963,TEMP, 533.
D, 2964,TEMP, 544.
D, 2965,TEMP, 555.
D, 2966,TEMP, 566.
.
.
(Repeated Commands Not Shown.)
.
SFE, 337, 2,HFLU,1,R5.0
0.000000000E+00 0.000000000E+00 0.000000000E+00 0.000000000E+00
SFE, 338, 2,HFLU,1,R5.0
0.000000000E+00 0.000000000E+00 0.000000000E+00 0.000000000E+00
SFE, 351, 2,HFLU,1,R5.0
0.000000000E+00 0.000000000E+00 0.000000000E+00 0.000000000E+00
SFE, 352, 2,HFLU,1,R5.0
0.000000000E+00 0.000000000E+00 0.000000000E+00 0.000000000E+00
.
.
(Repeated Commands Not Shown.)
.
.
/GOPR

```

**Table 16: Transient Solution Commands**

```
ANTYPE, TRAN, NEW  
/OUTPUT, (filename), RTH  
OUTPR, ALL, ALL  
OUTRES, ALL, ALL  
LSSOLVE, (initial load step number), (final load step number), 1
```

Figure 22: Temperature Contours at 240 Seconds

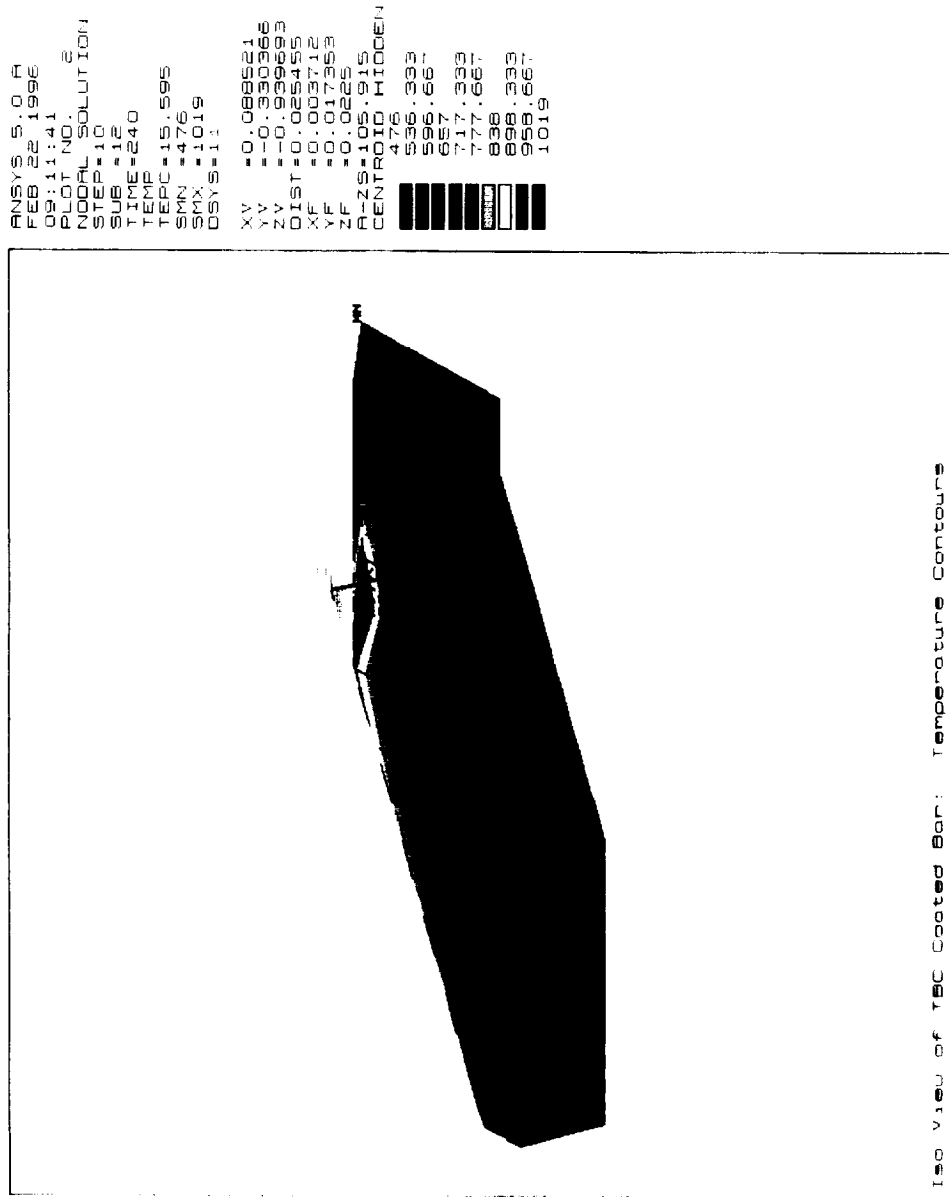
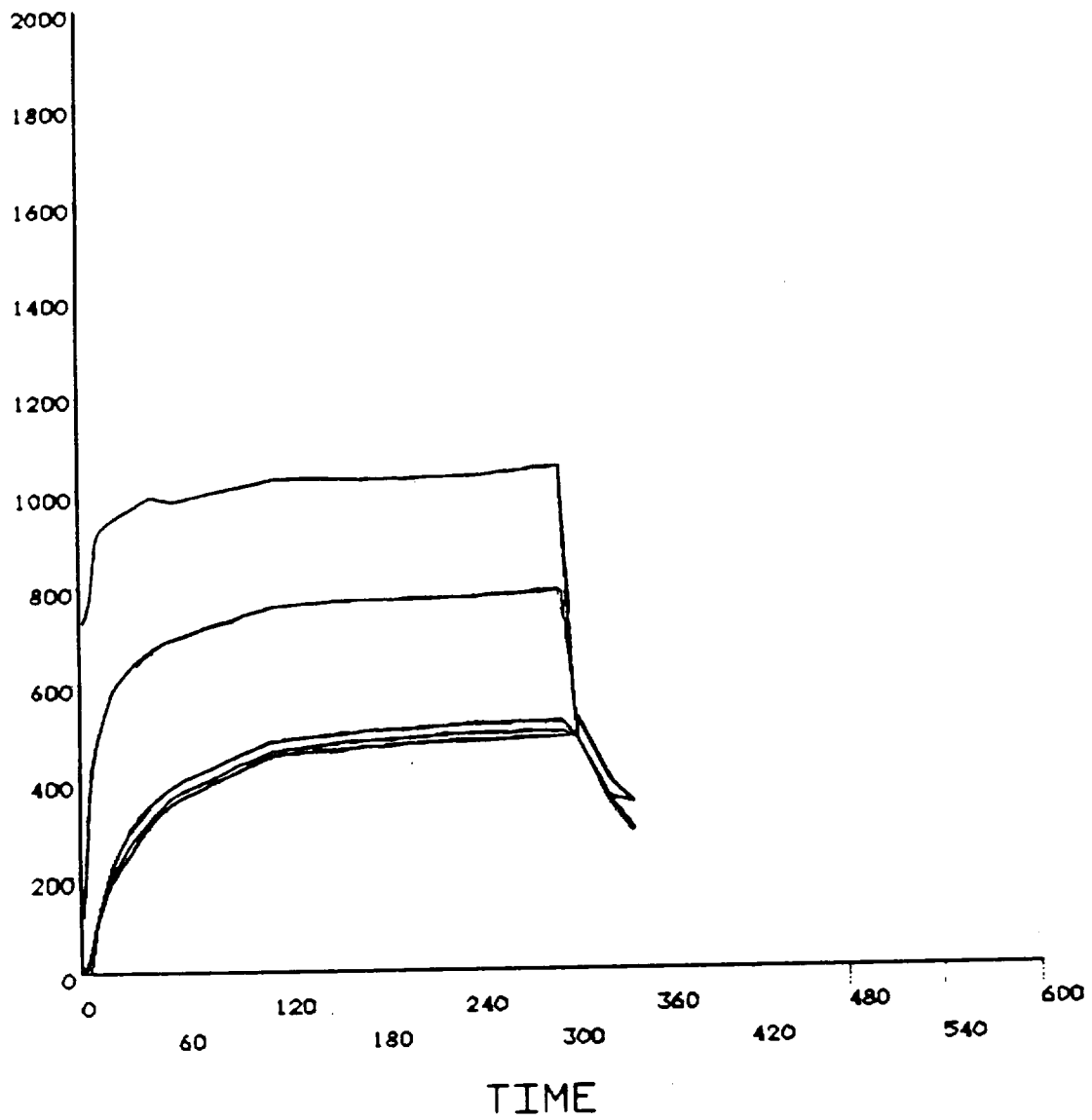
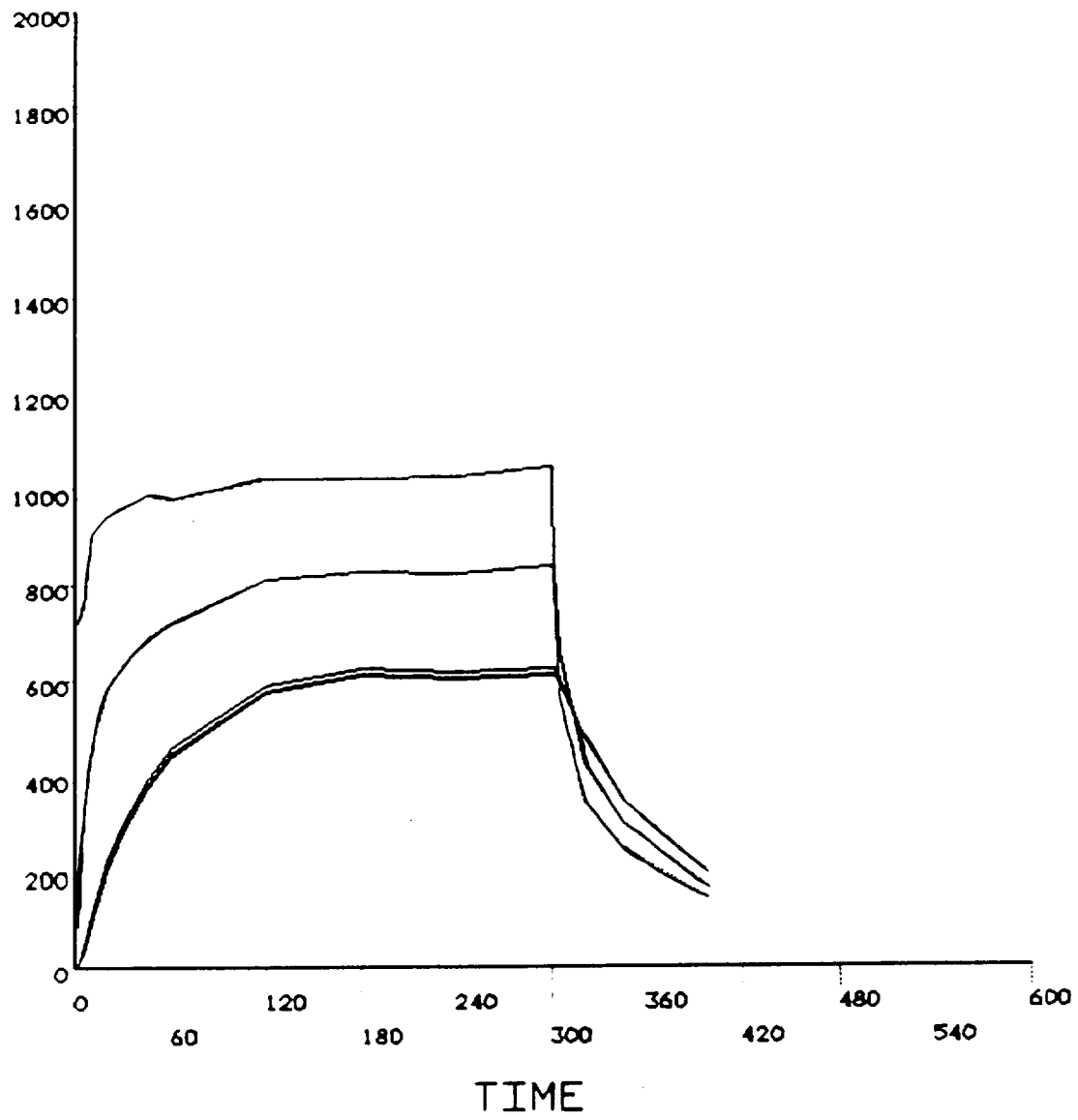


Figure 23: Non-convecting Model Temperatures vs. Time



**Figure 24: Convecting Model Temperatures vs. Time**



**Figure 25: Finite Element Model of Adhesion Pull-bar**

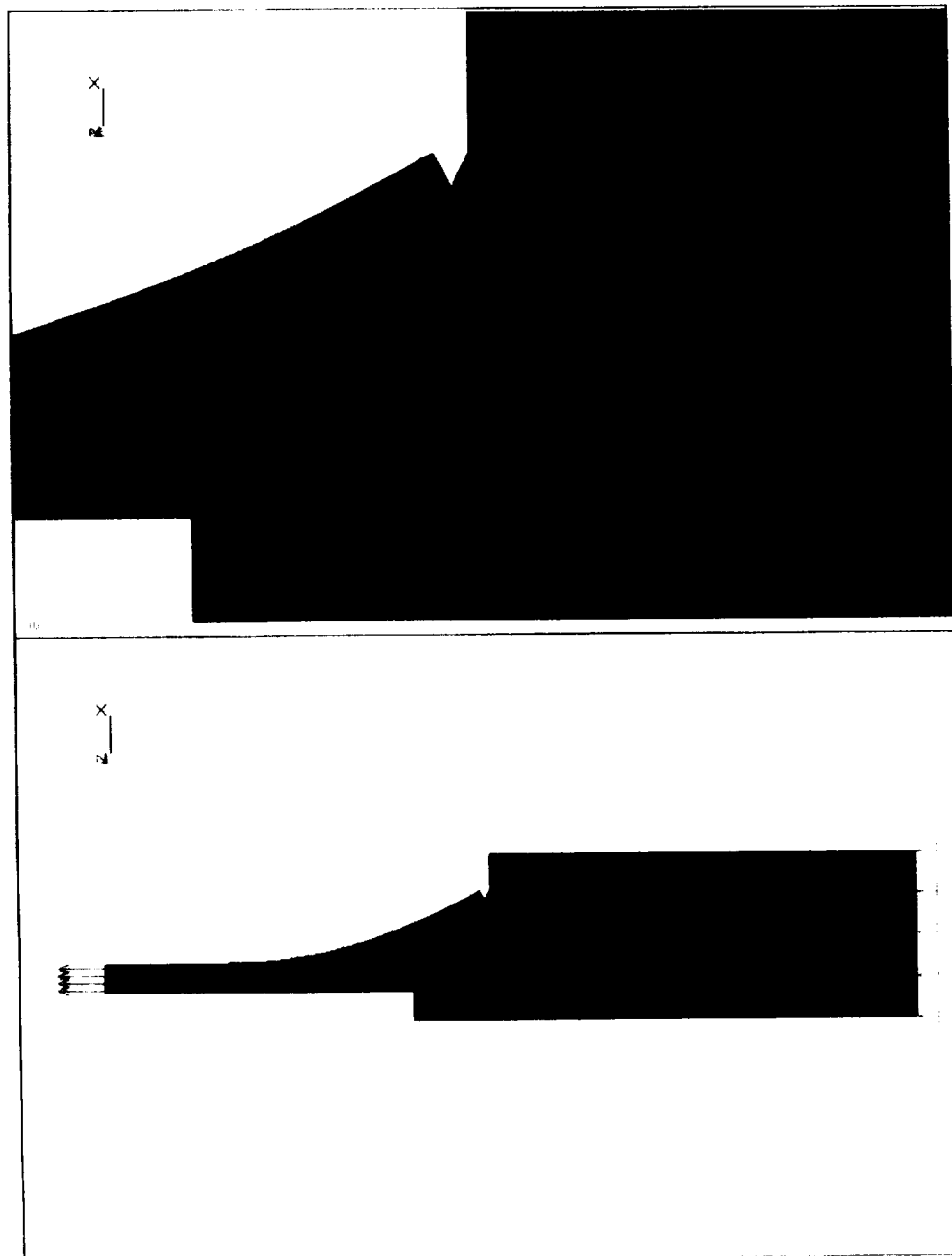


Table 17: Sample Input File for Adhesion Pull-bar Analysis

```

/BATCH
/COM,ANSYS REVISION 5.0 A 11:05:32
12/15/1994
/INPUT,START,ANS,D:\ANSYS50A\DOCU\
FILNAM.RUN_16
/TITLE,TBC PULL BAR: RUN 16
/PREP7
ET,1,PLANE82,,,1
MP,EX,1,30e6
MP,EX,2,1.96e6
MP,NUXY,1,.3
MP,NUXY,2,.13
K,1,0,0
K,2,0.433,0
K,3,0,1
K,4,0.433,1
K,5,0,1.01
K,6,0.433,1.01
K,7,0,1.06
K,8,0.333,1.06
K,9,0.433,1.06
K,10,0.333,1.085
K,11,0.075,2.06
!K,91,0.23,1.31
!K,92,0.165,1.56
!K,93,0.15,1.81
K,12,0.15,2.06
K,50,0,1.26
K,51,0.075,1.26
K,62,0.308,1.0725
L,1,2
L,1,3
L,2,4
L,3,4
L,3,5
L,4,6
L,5,6
L,5,7
L,6,9
L,7,8
L,8,9
L,7,50
L,8,62
L,11,12
!BSPLIN,10,91,92,93,12,.0
L,10,12
L,50,51
L,51,11
L,62,10
AL,1,2,3,4
AL,4,5,7,6
AL,7,8,10,11,9
AL,10,12,16,17,14,15,18,13
/AUTO
AGLUE,1,2
AGLUE,2,3
AGLUE,3,4
KSCON,8,0.001
LESIZE,8,,,4
LESIZE,9,,,4
LESIZE,14,,,4
LESIZE,5,,,1
LESIZE,6,,,1
MAT,1
AMESH,1
AMESH,2
AMESH,4
MAT,2
AMESH,3
FINISH
/SOLU
ANTYPE,0
DL,1,1,SYMM
SBCTRAN
SFL,14,PRES,-6572

```

```

SFTRAN
OUTPR,ALL
OUTRES,ALL
SAVE
SOLVE
FINISH
/POST1
SET
PLNSOL,S,Y

```

## References

- <sup>1</sup> ANSYS User's Manual For Revision 5.0, Volume III, Elements, Swanson Analysis Systems, Inc., 1993, pp. 4-455 - 4-458.
- <sup>2</sup> ANSYS User's Manual For Revision 5.0, Volume III, Elements, pp. 4-477 - 4-482.
- <sup>3</sup> Cruse, T. A., Personal Document: "NASA Thermal Barrier Coated Angle Iron Analysis", Volumes I and II, Vanderbilt University, 1994.
- <sup>4</sup> ANSYS User's Manual For Revision 5.0, Volume I, Procedures, Swanson Analysis Systems, Inc., 1993, pp. 10-2 - 10-5.
- <sup>5</sup> Mills, A. F., Heat Transfer, Homewood, Illinois: Irwin, 1992, p. 21.
- <sup>6</sup> Mills, p. 21.